Etchant and probabilistic ballistic models of diamond growth

M. Itoh, R. Sahara, M. Takahashi, X. Hu, K. Ohno, and Y. Kawazoe
Institute for Materials Research, Tohoku University, Sendai 980-77, Japan
(Received 13 July 1995)

Ballistic models of diamond growth in two-dimensional space are studied in detail. A probabilistic model is introduced to simplify and reduce computation, and is successfully compared with the etchant model, which was proposed recently by Capraro and Bar-Yam [Comput. Mater. Sci. **1**, 169 (1993)]. The growth process is shown to be divided into three distinct stages, and the limit of the expected thickness of the diamond film is indicated. The relation between the incident angle and growth direction is discussed. Analytic equations for the density of the resulting pattern are given, and a scaling analysis is performed.

PACS number(s): 05.40.+j, 68.35.Fx, 68.55.Jk

I. INTRODUCTION

To understand a growth process of nonuniform crystals by molecular beam epitaxy (MBE) or chemical vapor deposition (CVD), ballistic deposition models [1] have been proposed and successfully studied by computer simulations by Meakin [2], Family and Vicsek [3], Liang and Kadanoff [4], and others. In the original ballistic model, particles fall one by one from randomly selected starting points to the substrate perpendicularly, and are trapped on the growing object at which they first touch. This situation is thought to be typical for the particles in a low density gas and for the adsorption of particles with almost no surface diffusion. Associated continuum theories have been proposed by Ball and Witten [5], and by Kardar, Parisi, and Zhang (KPZ) [6], which describe the evolution and roughness of an interface. One simple extension of this original model is to change the incident angle of the particles from 0 to some value θ, and to study the dependence of the resulting pattern on this angle θ. The growth structure is generally columnar, starting from the substrate. Experimentally, an empirical formula for the relation between the direction of growth ζ and the direction of incident particles θ,

$$\tan\zeta \simeq \tfrac{1}{2}\tan\theta \ , \tag{1}$$

has been proposed [7] and investigated [8]. Relation (1) is known as the "tangential rule." The reliability of this rule has been discussed from the viewpoint of the ballistic model [9].

Recently a number of experimental studies have been performed on diamond synthesis from the gas phase. It utilizes a segregation process of carbon atoms from the dissociation of such gases as methane, ethane, alcohols, carbon monoxide, etc., and small particles and thin films can be obtained [10–13]. (For an *ab initio* calculation, see Ref. [14].) An epitaxial growth is achieved on the diamond substrate. The maximum thickness of the resulting diamond is around 100 Å. Surface diffusion of carbon atoms on the diamond (111) surface is known to be small. Therefore, this situation offers a typical example of a system to which the ballistic model can be applied. To simulate the effect of hydrogen or oxygen in gases of the diamond growth process, Capraro and Bar-Yam [15] introduced a procedure for etching in the ballistic model, and obtained various growth patterns. They assumed that, in addition to normal particles corresponding to carbon particles, etchant particles such as hydrogen or oxygen would also fall onto the substrate randomly. (The incident angle of all particles was assumed to be 0 for simplicity). We call this model the etchant ballistic model (EBM). The EBM differs from the standard ballistic model [2,9] or the solid-on-solid model [16] even in the absence of etchant particles, because the EBM allows corner-to-corner adsorption rather than side-by-side adsorption, in addition to the usual on-top adsorption; see Fig. 1(a). Thus the resulting patterns also are different from the standard model.

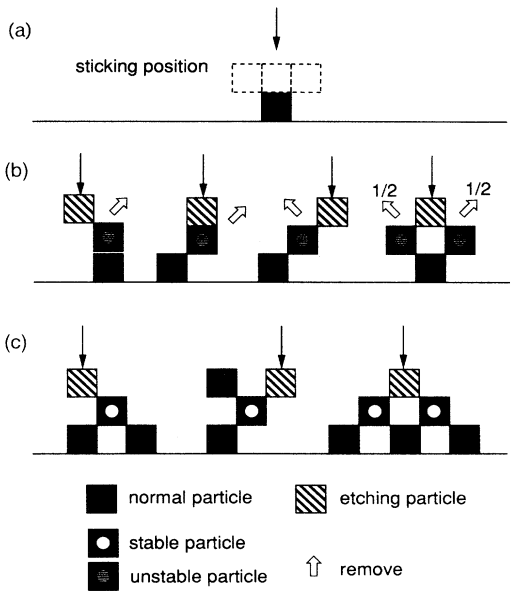

FIG. 1. Etchant ballistic model: (a) shows possible places at which normal particles can stick; (b) shows unstable particles (square marked with circle), which are removed by the etching particles, while (c) shows particles that are stable against etching.

In the EBM, a topmost normal particle attached to the surface only at lower-left or lower-right corner positions is removed, if an etchant particle falls on top or on upper corners of the attached normal particle. The topmost normal particle attached bottom on top to the surface particle without other contacts is also removed by etchant. The processes are illustrated in Fig. 1: Fig. 1(a) shows the possible places at which normal particles can stick. Figure 1(b) shows the unstable particles (square marked with circle) which are removed by the etching particles, while Fig. 1(c) shows the particles that are stable against etching. The etching process makes the growth process much slower, and the time required for the computer simulation increases with the ratio of the number of etchant particles to the number of normal particles E/N. Although the EBM reproduces typical characteristics of the diamond growth process in the gas phase, it has the following two disadvantages: (i) the process is complicated because of the introduction of etchant particles, and (ii) the simulation requires extensive computer time.

In the present paper we propose a probabilistic model which has a sticking probability p (see Fig. 2), instead of introducing etchant particles. We discuss the similarity of the resulting pattern of the EBM with this ballistic model, which we call the probabilistic ballistic model (PBM). This model reduces the computational time dramatically, because the number ratio of the etchants to the normal particles, E/N, is sometimes very high in the EBM. We shall show the results for PBM in the present paper. In order to make a complete discussion of the resulting patterns, we shall derive several important results for the EBM.

The rest of this paper is organized as follows: the tangential rule and θ dependence of the density in the original model of the EBM in the absence of etchant particles are discussed in Sec. II. In this section several analytic arguments concerning the density are also presented. More general growth processes of the EBM and PBM are discussed in detail, respectively, in Secs. III and IV. A scaling analysis of surface morphology is given for both the EBM and PBM Sec. V. Section VI is devoted to a summary of this paper.

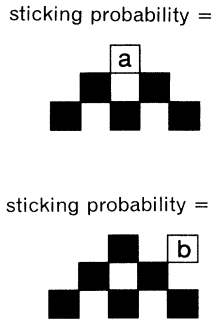

FIG. 2. Probabilistic ballistic model. A normal particle at the ith row sticks with a probability p, if the new height h_i' is the same as the height of neighbors h_{i-2} or h_{i+2}, and if only one of the lower corners is attached to an upper corner of a surface particle. If both of the lower corners are attached simultaneously, the normal particle sticks with a probability unity.

II. θ DEPENDENCES OF EBM WITHOUT ETCHING

In the simulations described in this and the next two sections, the length of the substrate is taken to be 200 meshes with periodic boundary conditions. To achieve good statistics, 100 samples are taken for each case.

Since Capraro and Bar-Yam's original model (EBM) with no etchant particles ($E/N=0$) is already different in sticking positions from the standard ballistic deposition model of Meakin [2,9], as is mentioned in Sec. I, it is worth deriving the incident angle θ dependences of the former model. First, in order to check the tangential rule, we study the growth direction of the columnar structures as a function of the incident angle θ of the particles (see Fig. 3). In place of the horizontal substrate and incident angle θ, we alternatively assumed the inclined substrate with the same angle θ against the horizon and vertical incidence of particles to the horizon. The results are shown in Fig. 4, where the solid straight line indicates the best fit to the function $C\tan\theta$: The best fit below 70° is $\tan\zeta=0.38\tan\theta$. The empirical tangential rule (1) holds, but the proportional constant is altered from $\frac{1}{2}$.

The next interesting quantity which, to our knowledge, has not been discussed previously is the packing density

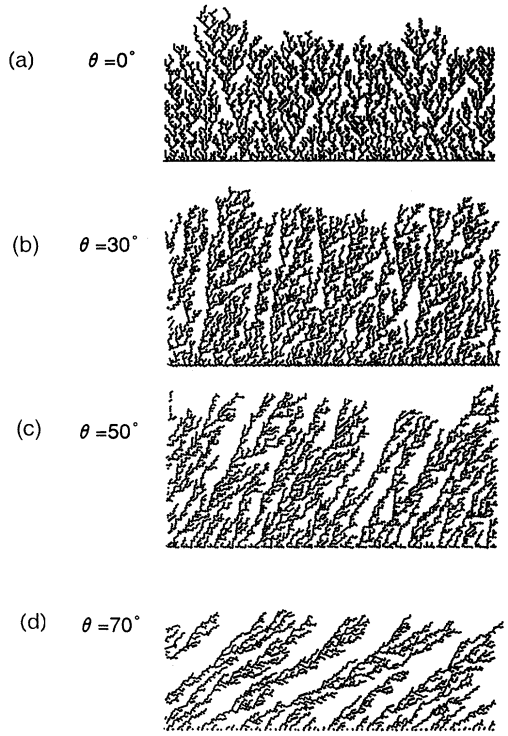

FIG. 3. Resulting patterns of Capraro and Bar-Yam's model without etchant particles for various incident angles (a) $\theta=0°$, (b) $\theta=30°$, (c) $\theta=50°$, and (d) $\theta=70°$.

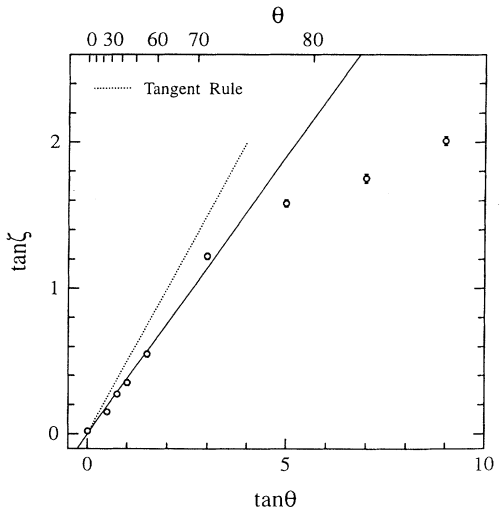

FIG. 4. Growing angle ζ vs incident angle θ (deg) of Capraro and Bar-Yam's model without etchant particles. The solid straight line indicates the behavior $\tan\zeta = C\tan\theta$ with a proportional constant $C = 0.38$. The dashed straight line corresponds to $C = 0.5$ in Eq. (1).

of the resulting pattern. The packing density ρ is plotted as a function of the incident angle θ in Fig. 5. For $\theta = 0$, the density is close to 0.25, while for larger θ the density decreases gradually toward 0 at $\theta = \pi/2$. In order to understand this behavior of the density, we performed some simple analytic considerations.

First, the density of the pattern in the case of $\theta = 0$ can be discussed by means of a simple mean-field argument. Suppose that the average density at a definite height is ρ. The probabilities for occupying and not occupying one site are ρ and $1-\rho$, respectively, provided that the correlations among neighboring sites are neglected. As shown in Fig. 6, if site 1 is occupied, site 2 should be vacant

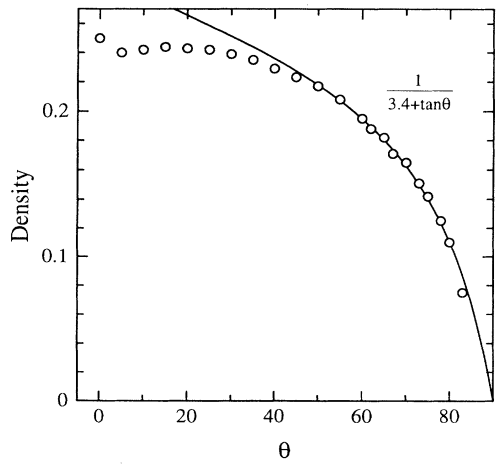

FIG. 5. θ dependence of the density of Capraro and Bar-Yam's model without etchant particles. The solid curve indicates the theoretical relation (11) with $a = 3.4$ and $b = 1.0$.

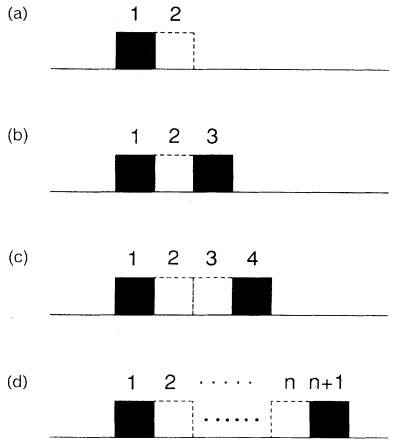

FIG. 6. Self-consistent picture in determining the monolayer packing density of the original ballistic model.

from the growth rule of the model, and the probability that the first occupation right to site 1 occurs at site 3 is ρ. The density for this configuration is $\frac{1}{2}$. The probability for the case where site 4 is the leftmost occupied site to site 1 is $\rho(1-\rho)$, associated with a density $\frac{1}{3}$. Similarly the probability for the case where site $(n+1)$ is the leftmost occupied site should be $\rho(1-\rho)^{n-2}$, and the density should be $1/n$. The density can then be evaluated by these exclusive events as

$$\tfrac{1}{2}\rho+\tfrac{1}{3}\rho(1-\rho)+\cdots+\frac{1}{n}\rho(1-\rho)^{n-2}+\cdots = \sum_{n=2}^{\infty}\frac{\rho(1-\rho)^{n-2}}{n} . \quad (2)$$

The density ρ is determined self-consistently by equating itself to the above estimation:

$$-\ln\rho-(1-\rho)(2-\rho) , \quad (3)$$

and is evaluated as $\rho = 0.316\,20$. In the above argument, fluctuation from the expectation value is neglected, which may play an important role via the over-hanger effect in dendritic growth [16].

In the following, we will derive another analytic equation for the density of the pattern as a function of the incident angle θ of the particles, which is now the slope of the inclined substrate to make simulation easier. In the model, growth is associated with the adsorption of particles as shown in Fig. 7. If a particle is adsorbed at site i, the height variable changes from h_i to h_i'. Here the height at time t is h_i, and that at time $t+\Delta t$ is h_i'. According to the particle attachment, it alters as

$$h_i' = h_i + 1,$$
$$h_{i+1}' = h_i + 1$$

for $h_i > h_{i+1}$, and

$$h_i' = h_{i+1} + 1,$$
$$h_{i+1}' = h_{i+1} + 1$$

for $h_i < h_{i+1}$. Introducing the step function Θ, which is expressed by the sgn function as $\Theta(x)=[1+\mathrm{sgn}(x)]/2$, we have

$$\begin{aligned} h_i' &= (h_i+1)\Theta(h_i-h_{i+1})+(h_{i+1}+1)\Theta(h_{i+1}-h_i)+\eta_i \\ &= \tfrac{1}{2}(h_i+h_{i+1})+\tfrac{1}{2}(h_i-h_{i+1})\mathrm{sgn}(h_i-h_{i+1})+1+\eta_i \\ &= \tfrac{1}{2}(h_i+h_{i+1})+\tfrac{1}{2}|h_i-h_{i+1}|+1+\eta_i \ , \end{aligned} \tag{4}$$

where η_i denotes a random force acting as a random selector of site variable i. Using a continuum approximation, we obtain, by setting $x=i\Delta x$,

$$h_i'-\tfrac{1}{2}(h_i+h_{i+1})=\frac{1}{2}\left|h_i-\left[h_i+\Delta x\frac{dh}{dx}\right]\right|+1+\eta, \tag{5}$$

where h and η are the functions of (x,t). From Eq. (5), we derive the equation

$$\frac{dh}{dt}\cong 1+\frac{\Delta x}{2}\left|\frac{dh}{dx}\right|+\eta \ , \tag{6}$$

which has a form similar to the generalized KPZ equation [17,18]. The only difference is the absence of the term proportional to $\nabla^2 h$ in our equation. [This difference is, however, not very important, since the term $\nabla^2 h$ is always relevant in the renormalization and its absence in Eq. (6) is just occasional.] Since we are considering the inclined substrate, we expect

$$\left\langle\left|\frac{dh}{dx}\right|\right\rangle\approx\tan\theta \ , \tag{7}$$

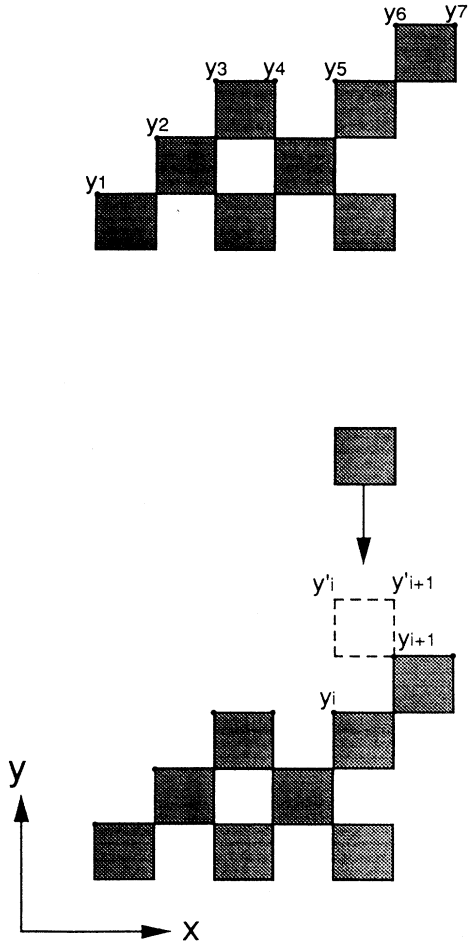

FIG. 7. Relation between a sticking position i and its height h_i in Capraro and Bar-Yam's model without etchant particles. The new height at time $t+\Delta t$ is indicated as h_i'.

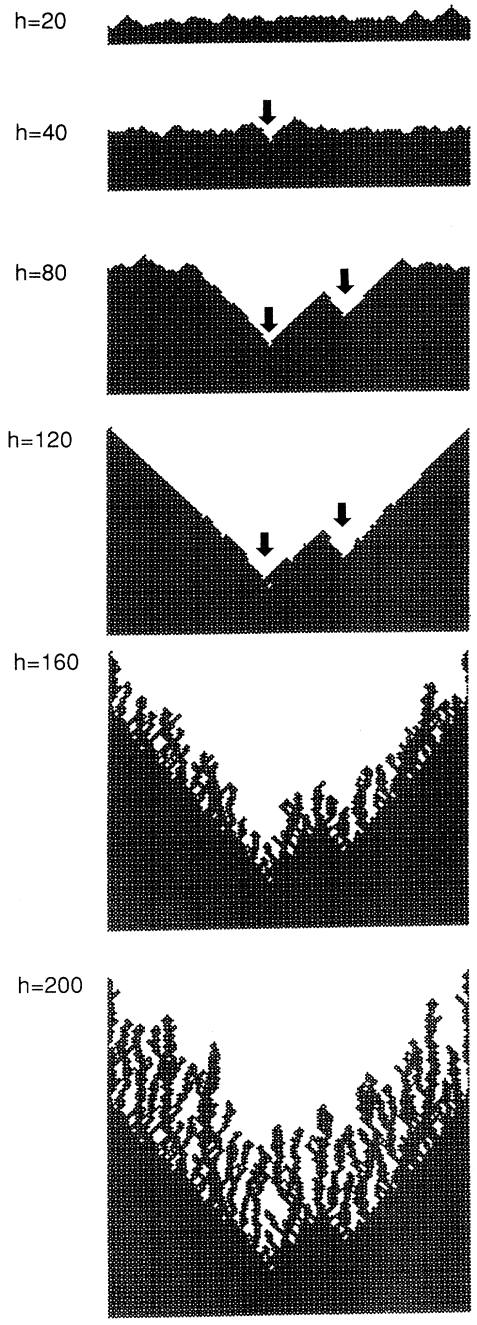

FIG. 8. Typical patterns of the EBM in the case $E/N=300$. Pictures correspond to several different growing stages with heights from $h=20$ to 200.

if the growth rate and in turn the average height from the substrate are both site independent. By taking an ensemble average of Eq. (6), we obtain

$$\left\langle \frac{dh}{dx} \right\rangle \cong 1+\frac{\Delta x}{2}\left\langle \left| \frac{dh}{dx} \right| \right\rangle + \langle \eta \rangle$$
$$\approx a + b \tan\theta \ . \tag{8}$$

Since the density ρ is proportional to $1/\langle dh/dt \rangle$, it is finally expressed as

$$\rho \propto 1 \Big/ \left\langle \frac{dh}{dt} \right\rangle = \frac{1}{a + b \tan\theta} \ . \tag{9}$$

The best fit is obtained with $a = 3.4$ and $b = 1.0$, as indicated by the solid curve in Fig. 5.

III. GROWTH PROCESS OF EBM

A typical growth process is shown in Fig. 8 for the value of $E/N = 300$. The value h in the figure indicates the highest point at the time. According to this result, we can classify the growth process into three stages. In the first stage, up to $h = 40$, an almost flat surface is maintained, and the resulting pattern is completely dense. The sites are almost all stable. In the second stage, up to $h = 120$, inclined facets with the angle of $\pm 45°$ appear. The surface is covered almost everywhere with these inclined facets with $\pm 45°$ at the end of this stage (at $h = 120$ in Fig. 8), and there remain almost no stable sites for new incident particles. In the third stage, after $h > 120$, columnar growths start. The growth of the structure becomes two orders of magnitude slower in the third stage compared to the first two stages. In Fig. 8, the arrows indicate the points at which the $\pm 45°$ facets nucleate to induce the columnar growth. We show the resulting patterns of different E/N values in Fig. 9. It is worth noting that the patterns of the columnar growth in the third stage are not sensitive to the value of E/N when E/N is somewhat larger than unity, cf. $E/N > 3$, which is surely due to the universality. This result will be discussed again in Sec. IV within the context of scaling.

The thickness of the industrially interesting diamond is considered to be related to the maximum height limit of the effective and the region of dense film formation in the second stage growth. The height limit of the second stage growth $H_{\rm lim}$ is indicated as a function of the E/N value in Fig. 10. On the other hand, the minimum height $H_{\rm min}$ in the second stage is comparable to the height at the beginning of the second stage. The minimum height $H_{\rm min}$ and the number of valleys $N_{\rm defect}$ are also shown versus E/N in the same figure, Fig. 10. Since $H_{\rm min}$ is related to the valley formation due to an accidental stabilization of the first defect, $H_{\rm min}$ is roughly proportional to E/N; see the dotted line in Fig. 10. Moreover, we found that $H_{\rm lim}$ can be fitted well by an equation

$$H_{\rm lim} = 10.5 \times (E/N)^{0.34} + 2, \tag{10}$$

which is depicted by the solid curve in Fig. 10, and that $N_{\rm defect}$ is proportional to the size L of the substrate: $N_{\rm defect} = 0.02 \times L$.

Next we consider the behavior of the density ρ in the EBM. The density as a function of E/N in the third

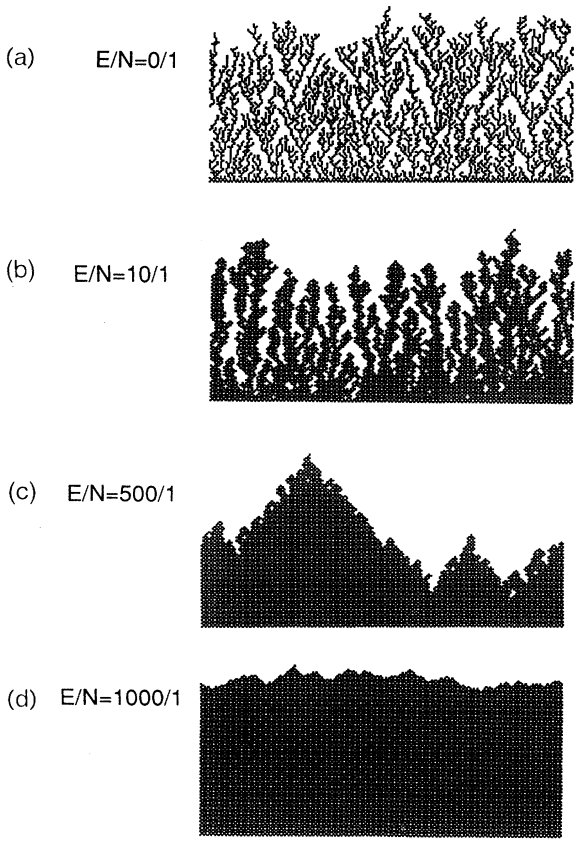

FIG. 9. Patterns of the EBM for different E/N values: (a) $E/N = 0$, (b) $E/N = 10$, (c) $E/N = 500$, and (d) $E/N = 1000$.

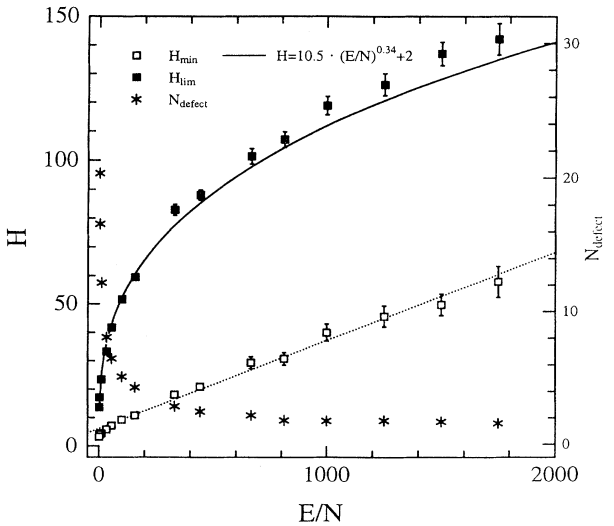

FIG. 10. E/N dependences of $H_{\rm lim}$ (the height limit in the dense region), $H_{\rm min}$ (the minimum height), and $N_{\rm defect}$ (the number of defects is equal to the number of valleys).

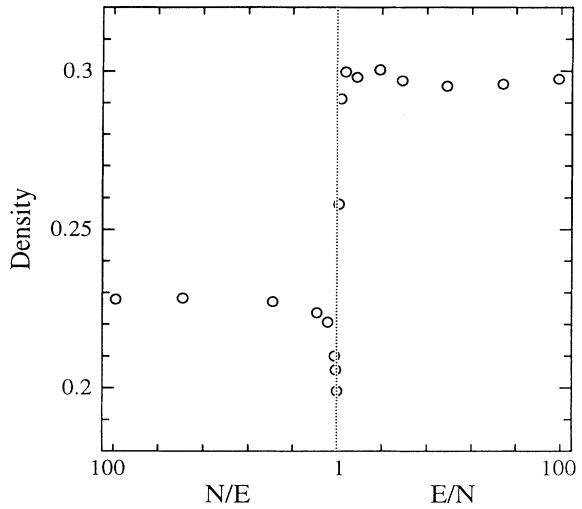

FIG. 11. E/N dependence of the density ρ of the EBM ($\theta=45°$) at the third stage. The right (left) hand side corresponds to the strong (weak) etching condition with $E/N>1$ ($E/N<1$). The density ρ jumps from its minimum value $\rho_{\min}=0.2$ to $\rho=0.3$ in the vicinity of $N/E=1$.

stage is shown in Fig. 11 in the case of $\theta=45°$. The right (left) hand side corresponds to the strong (weak) etching condition with $E/N>1$ ($E/N<1$). The center is located at $E/N=1$. We know that $\rho\sim0.23$ in the limit $E/N\to0$. If we go from small E/N to large E/N in the figure, the density ρ decreases gradually around $N/E=10$, and has a minimum $\rho_{\min}=0.20$ at $N/E=1$. Then it suddenly jumps to $\rho=0.30$, and remains constant for $E/N>1$. It is interesting to note that $\rho=0.30$ for $E/N>1$ is rather close to the value obtained from Eq. (3), although this coincidence might be accidental. The abrupt change of the density at $E/N=1$ is also very interesting, but its detailed analysis is left for future study.

The required number of incident particles, $N(h)$, to achieve the average height h, say $h=100$, is shown in Fig. 12. This number depends strongly on E/N. The increment of $N(h)$ as a function of E/N is faster than a single exponential, and effectively no film growth is expected for large E/N.

Before ending this section, we briefly comment on the pattern in the EBM, when we change the incident angle θ from 0 to finite values. Figure 13 (see also Fig. 11) shows a typical example in the case $\theta=\pi/4$. Clearly, the growing angle ζ coincides with the incident angle θ for E/N *somewhat greater than unity.* This is probably due to the weakness of the screening effect in the EBM. Although we do not present the result here explicitly, the same behavior is also observed in the PBM.

IV. GROWTH PROCESS OF PBM

In the PBM, as shown in Fig. 2, particles are not allowed to stick either bottom on top or side by side with surface particles, but stick with probability unity if both lower-left and lower-right corners are attached simultaneously to upper corners of surface particles. Moreover, a

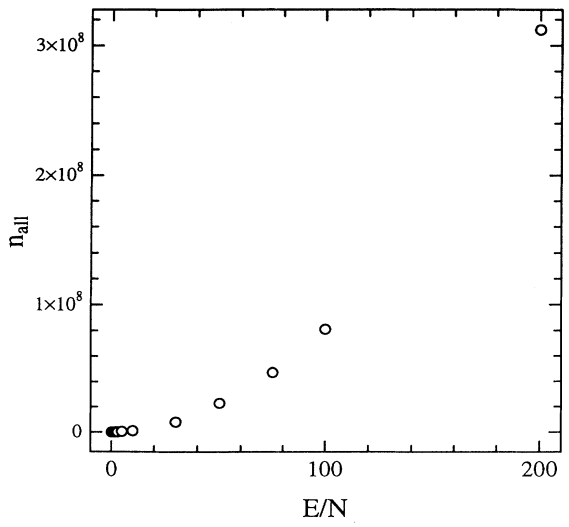

FIG. 12. Number of normal particles $n_{\text{all}}=N(h)$, required for growing the objects to a given height h in the EBM ($h=100$).

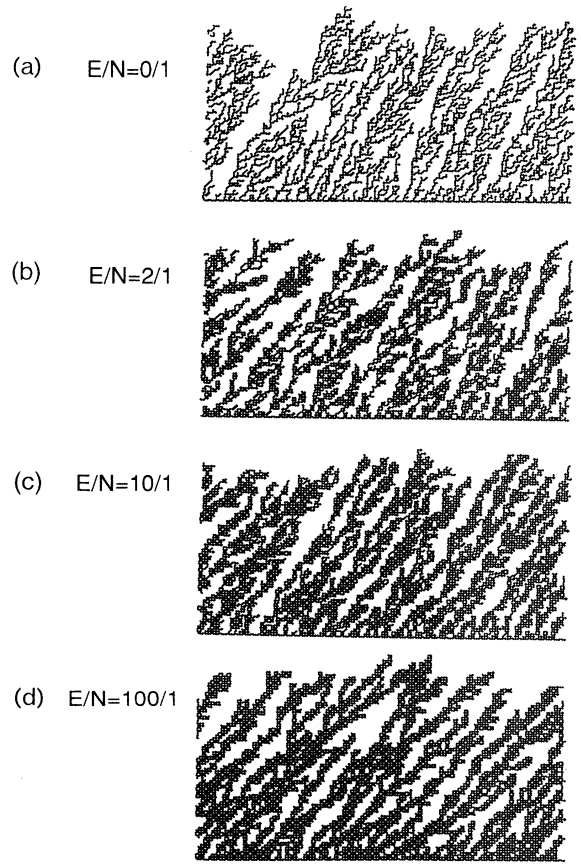

FIG. 13. Patterns obtained for the case of incident angle $\theta=45°$ for various values of E/N: (a) $E/N=0$, (b) $E/N=2$, (c) $E/N=10$, and (d) $E/N=100$.

normal particle at the ith row sticks with probability p, if the new height h_i' is the same as the height of neighbors h_{i-2} or h_{i+2}, *and* if only one of the lower corners is attached to an upper corner of a surface particle. Thus only checkerboard positions can be occupied, if the substrate is constructed commensurately with a single uniform checkerboard pattern. In such a model, one can obtain results similar to those of the EBM expect for the case $E/N \leq 1$. In Fig. 14, we show typical results of the PBM for various values of p. The probability p in the PBM is related to the ratio of the number of etchant particles to the total number of particles, $p_{\text{normal}} = N/(N+E)$, in the EBM, if E/N is somewhat greater than unity:

$$p = \frac{p_{\text{normal}}}{3} = \frac{N}{3(N+E)} . \tag{11}$$

Except for (a) violating $p \ll 1$, all the patterns in Fig. 14 are extremely similar to those obtained in the EBM with $p = N/3(N+E)$. For $E/N \gg 1$ (or $p \ll 1$), both models show an abrupt change of patterns at some height from checkerboard (dense) growth to dendritic growth. For comparison, the pattern obtained by the EBM with $E/N = 5$ and the corresponding pattern obtained by the PBM with $p = \frac{1}{18}$ are shown in Fig. 15. They are very similar to each other and it is actually impossible to distinguish these two patterns.

Relation (11) is derived as follows; see Fig. 16. Suppose

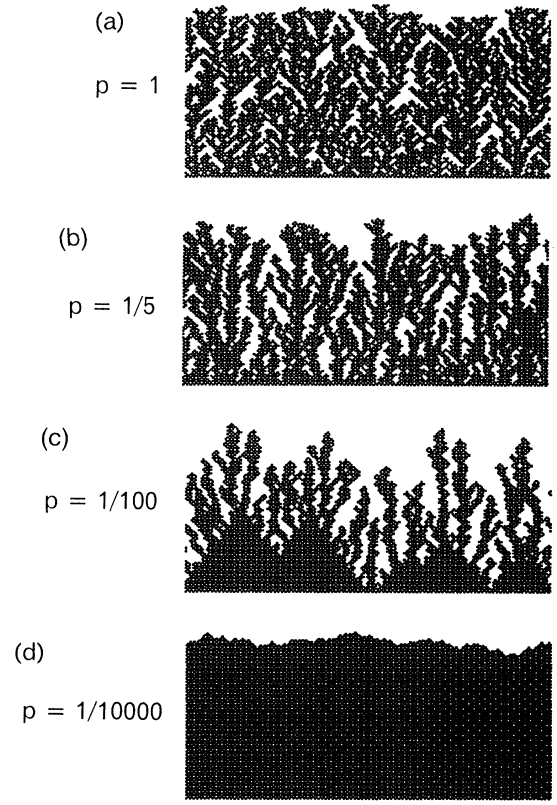

FIG. 14. Typical patterns of the PBM with different probabilities (a) $p = 1$, (b) $p = \frac{1}{5}$, (c) $p = \frac{1}{100}$, and (d) $d = \frac{1}{10000}$.

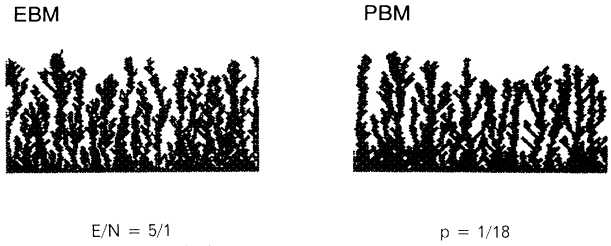

FIG. 15. Patterns obtained in the EBM with $E/N = 5$ and the PBM with $p = \frac{1}{18}$.

that an unstable particle attached at a position A is stabilized by another particle attached at a position B at the mth step after A is attached. The probability of this event p_m is estimated as

$$p_m = \left[1 - \frac{3}{L}p_{\text{etchant}} - \frac{1}{L}p_{\text{normal}}\right]^{m-1} \frac{1}{L}p_{\text{normal}}, \tag{12}$$

where $P_{\text{etchant}} = E/(N+E)$. From this equation, the probability P_m that position A *is stable* after m steps from its adsorption is given by the equation

$$P_m = \sum_{n=1}^{m} p_n \sim \frac{p_{\text{normal}}}{3} \tag{13}$$

for $m \geq L$. Here, we assumed that L is large enough and $p_{\text{normal}} \ll p_{\text{etchant}}$. Since $p = \lim_{m\to\infty} P_m$, we derive the desired equation (11).

V. SCALING ANALYSIS

In order to show that the patterns obtained by the EBM and PBM belong to the same universality class, we

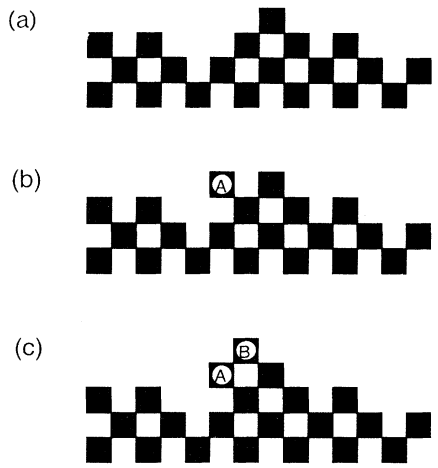

FIG. 16. Illustration for the derivation of Eq. (13) between p and $p_{\text{normal}} = N/(N+E)$. Position A is stabilized by the second incident particle at position B; (a) is the original surface, (b) the surface with one particle adsorbed at position A, and (c) the surface with another particle adsorbed at position B which stabilizes particle A.

analyze the fractal nature of the growing surface. We introduce the parameter $\sigma(L,h)$ defined by

$$\sigma(L,h)=\left[\frac{1}{N_s}\sum_{i=1}^{N_s}(h_i-h)^2\right]^{1/2},$$
$$h=\frac{1}{N_s}\sum_{i=1}^{N_s}h_i, \tag{14}$$

where N_s is the number of lattice points at the surface, L the width of the periodic boundary condition, and h_i the height of the structure at the ith lattice from the substrate. For dendritic or columnar growths, there are two scaling regions in general. One is for $h \ll L$, where fluctuations in the surface grow as a power of h. Another is for $h \gg L$, where the surface is stable and the typical width does not depend on h. The scaling equation is

$$\sigma(L,h)\sim L^{\alpha} f\left[\frac{h}{L^z}\right], \tag{15}$$

where the scaling function $f(x)$ behaves as

$$f(x)\sim\begin{cases} x^{\beta}, & x \ll 1 \\ \text{const}, & x \gg 1 \end{cases} \tag{16}$$

and

$$\sigma(L,h)\sim\begin{cases} h^{\beta}, & h/L^z \ll 1 \\ L^{\alpha}, & h/L^z \gg 1, \end{cases} \tag{17}$$

with $z=\alpha/\beta$. The best fitted values of α and β are

$$\begin{aligned} &\text{for } E/N=0/1, \quad \alpha=0.49\pm0.08, \quad \beta=0.31\pm0.05, \\ &\text{for } E/N=5/1, \quad \alpha=0.95\pm0.08, \quad \beta=0.35\pm0.05. \end{aligned} \tag{18}$$

The values for $E/N=0$ should be compared with those of the standard ballistic model [2,9]; the latter is considered to be in the same universality class as the KPZ equation [6]. In two dimensions, the scaling exponents for the KPZ equation have been determined using renormalization-group analysis [6,19,20,21] and symmetry arguments [22] to be $\alpha=\frac{1}{2}$ and $\beta=\frac{1}{3}$. These values are indeed consistent with our data within the estimated error. On the other hand, the values for the third stage growth for $E/N=5/1$ and of course nontrivial, and should be compared to those of the PBM with $p=N/3(N+E)$. For such a PBM (see Fig. 15), we obtain α and β as

$$\text{for } p=\tfrac{1}{18}, \quad \alpha=1.08\pm0.08, \quad \beta=0.32\pm0.05, \tag{19}$$

which coincides with the values of the EBM in the case $E/N=5/1$ within the error of estimates. We believe that the EBM with $E/N \gg 1$ and the PBM with $p \ll 1$ belong to the same universality class in the third stage growth, and the corresponding universal exponents are $\alpha\sim 1$ and $\beta\sim 1/3$.

VI. SUMMARY

Ballistic models of diamond growth have been studied in detail. The effect of the etchant particles in the growth process has been analyzed in Capraro and Bar-Yam's model (EBM). Moreover, a probabilistic model (PBM) for selective attachment of particles instead of etching was introduced, and this model successfully reproduces the EBM results with a significant reduction of computational time. The growth process is clearly divided into three stages: perfect growth in the first stage; the second stage, in which large facets are still available; and the third stage of very slow and complex growth.

Analytic evaluation is performed for the density of growth patterns, and coincidence with the simulation of strong etching is obtained. An expression has been obtained for the density of the resulting material as a function of the incident angle of particles. The validity of this expression of large angles was proved by comparing with numerical results.

ACKNOWLEDGMENTS

The authors are grateful to the continuous support of the computing facility by the Computer Science Group at Institute for Materials Research, Tohoku University. They are also thankful for Dr. Marcel Sluiter for his careful reading of the manuscript. One of the authors (K.O.) acknowledges support by the Mazda Foundation and by the Grant-in-Aid for Science Research (Synthetic Research A) on "Quantum Theory and Structural Dynamics of Epitaxial Growth" from the Ministry of Education, Science and Culture of Japan.

[1] T. Vicsek, *Fractal Growth Phenomena,* 2nd ed. (World Scientfic, Singapore, 1992), Chaps. 7 and 12.
[2] P. Meakin, J. Phys. A **18**, L661 (1985); J. Colloid Interface Sci. **105**, 240 (1985).
[3] F. Family and T. Vicsek, J. Phys. A **18**, L75 (1985).
[4] S. Liang and L. P. Kadanoff, Phys. Rev. A **31**, 2628 (1985).
[5] R. C. Ball and T. A. Witten, Phys. Rev. A **29**, 2966 (1984); J. Stat. Phys. **36**, 873 (1984).
[6] M. Kardar, G. Parisi, and Y. Zhang, Phys. Rev. Lett. **56**, 889 (1986).
[7] J. M. Nieuwenhuzzen and H. B. Haanstra, Philips Tech. Rev. **27**, 87 (1966).
[8] H. J. Leamy, G. M. Gilmer, and A. G. Dirks, *Current Topics in Material Science* (North-Holland, Amsterdam, 1980), Vol. 6, p. 309.
[9] P. Meakin, Phys. Rev. A **38**, 994 (1988).
[10] B. V. Spitsyn, L. L. Bouilov, and B. V. Derjaguin, J. Cryst. Growth **52**, 219 (1981).
[11] R. C. A. De Vries, Rev. Mater. Sci. **17**, 161 (1987).
[12] J. C. Angus and C. C. Hayman, Science **241**, 913 (1988).
[13] A. R. Badzian, and R. C. De Vries, Mater. Res. Bull. **23**, 385 (1988).
[14] M. Tsuda, M. Nakajima, and S. Oikawa, J. Am. Chem. Soc. **108**, 5780 (1986).

[15] C. T. Capraro and Y. Bar-Yam, Comput. Mater. Sci. **1**, 169 (1993).
[16] M. Siegert and M. Plischke, Phys. Rev. E **50**, 917 (1994).
[17] J. Krug and H. Spohn, Phys. Rev. A **38**, 4271 (1988).
[18] J. G. Amar and F. Family, Phys. Rev. E **47**, 1595 (1993).
[19] D. Forster, D. R. Nelson, and M. J. Stephen, Phys. Rev. A **16**, 732 (1977).
[20] E. Medina, T. Hwa, M. Kardar, and Y. Zhang, Phys. Rev. A **39**, 3053 (1989).
[21] T. Sun and M. Plischke, Phys. Rev. E **49**, 5046 (1994).
[22] D. A. Huse, C. L. Henley, and D. S. Fisher, Phys. Rev. Lett. **55**, 2924 (1985).